Accumulation and Photocytotoxicity of Hypericin and Analogs in Two- and Three-Dimensional Cultures of Transitional Cell Carcinoma Cells

Author(s): Ann Huygens, Dieter Huyghe, Guy Bormans, Alfons Verbruggen, Appolinary R. Kamuhabwa, Tania Roskams, and Peter A. M. de Witte

Source: Photochemistry and Photobiology, 78(6):607-614.
Published By: American Society for Photobiology
DOI: http://dx.doi.org/10.1562/0031-8655(2003)078<0607:AAPOHA>2.0.CO;2
URL: http://www.bioone.org/doi/full/10.1562/0031-8655%282003%29078%3C0607%3AAAPOHA%3E2.0.CO%3B2

Photochemistry and Photobiology, 2003, 78(6): 607–614

Accumulation and Photocytotoxicity of Hypericin and Analogs in Two- and Three-Dimensional Cultures of Transitional Cell Carcinoma Cells¶

Ann Huygens[1], Dieter Huyghe[2], Guy Bormans[2], Alfons Verbruggen[2], Appolinary R. Kamuhabwa[1], Tania Roskams[3] and Peter A. M. de Witte*[1]

[1]Laboratorium voor Farmaceutische Biologie en Fytofarmacologie, Faculteit Farmaceutische Wetenschappen, Katholieke Universiteit Leuven, Leuven, Belgium;
[2]Laboratorium voor Radiofarmaceutische Chemie, Faculteit Farmaceutische Wetenschappen, Katholieke Universiteit Leuven, Leuven, Belgium and
[3]Afdeling Histochemie en Cytochemie, Faculteit Geneeskunde, Katholieke Universiteit Leuven, Leuven, Belgium

Received 2 July 2003; accepted 5 September 2003

ABSTRACT

The aim of this study was to investigate the *in vitro* cellular accumulation, distribution and photocytotoxic effect of hypericin in two-dimensional (2-D) and three-dimensional (3-D) cultured RT-112 transitional cell carcinoma cells of the bladder. In addition, two iodinated derivatives of hypericin were incorporated to investigate whether these analogs, with their increased lipophilicity and heavy–atom effect, display a different biological behavior and optimized photodynamic effect. The results indicate that hypericin and mono–iodohypericin behave similarly in terms of cellular accumulation, spheroidal distribution and photocytotoxic effect. In contrast, di-iodohypericin concentrated to a higher extent in monolayers and spheroids, but the accumulation was restricted to the outermost part of the spheroid. An inverse correlation therefore seems to exist between the extent of cellular uptake under 2-D conditions and the penetration of the compounds in multicellular systems. Moreover, a less pronounced photocytotoxic effect was observed for di-iodohypericin in both 2-D and 3-D cell culture systems. It can be concluded that iodinated derivatives of hypericin do not show an increased cytotoxic effect upon irradiation in either monolayers or spheroids. Moreover, this study shows that when new photosensitizers are preclinically developed, the use of 3-D cell aggregates is critical for a correct evaluation of their efficacy.

INTRODUCTION

Photodynamic therapy (PDT) of cancer is based on the local or systemic administration of a photosensitizer that accumulates preferentially in tumor tissue. Illumination of the tumor with light matching the absorption maximum of the photosensitizer leads to an electronically excited molecule. For a photodynamic effect to take place the photosensitizer should subsequently undergo intersystem crossing into its long-lived triplet state, resulting in photochemical reactions that generate tumoricidal reactive oxygen species (ROS) like singlet oxygen (1,2). Second-generation photosensitizers with improved characteristics and enhanced PDT efficacy are under development in many laboratories (3–5). Such photosensitizers should be chemically pure, absorb light of a wavelength between 600 and 850 nm and possess photophysical properties that are conducive for generating ROS efficiently. Because of its potent photosensitizing characteristics, we and other investigators have been focusing on hypericin as a novel PDT tool in the treatment of cancer (6–11). Hypericin is a hydroxylated phenanthroperylenequinone present in a number of plants of the genus *Hypericum*, widely distributed around the world, the most common of which is *H. perforatum* (12). It is capable of generating singlet oxygen efficiently (13–16) and, to a smaller extent, also superoxide radicals (17).

By means of fluorescence-guided cystoscopy, we have shown previously that hypericin localizes very selectively in transitional papillary carcinoma and flat carcinoma *in situ* (CIS) after intravesical administration of the compound in patients (18,19). Because hypericin is a potent photosensitizer, its specific localization in early-stage urothelial carcinoma lesions of the bladder offers a unique opportunity not only to detect but also to treat the tumor lesions photodynamically. Therefore, PDT of superficial urinary bladder cancer with hypericin looks very promising. Presently, however, no data are available that describe in more detail the tumoritropic behavior of hypericin. For instance, it is not known to what extent the lipophilic–hydrophilic character

¶Posted on the website on 28 September 2003

*To whom correspondence should be addressed at: Laboratorium voor Farmaceutische Biologie en Fytofarmacologie, Faculteit Farmaceutische Wetenschappen, Katholieke Universiteit Leuven, Van Evenstraat 4, B-3000 Leuven, Belgium. Fax: 32-16-323460; e-mail: peter.dewitte@pharm.kuleuven.ac.be

Abbreviations: ANOVA, analysis of variance; CIS, carcinoma *in situ;* DMSO, dimethylsulfoxide; ECM, extracellular matrix; GAG, glycosaminoglycan; FCS, fetal calf serum; LDL, low-density lipoproteins; MEM, minimum essential medium; MPLC, medium–performance liquid chromatography; MTT, 3-(4,5-dimethylthiazol-2-yl)-2,5-diphenyl-tetrazolium bromide; PBS, phosphate-buffered saline; PDT, photodynamic therapy; ROS, reactive oxygen species; RP-HPLC, reversed phase high-performance liquid chromatography; SD, standard deviation; TCC, transitional cell carcinoma; 2-D, two-dimensional; 3-D, three-dimensional.

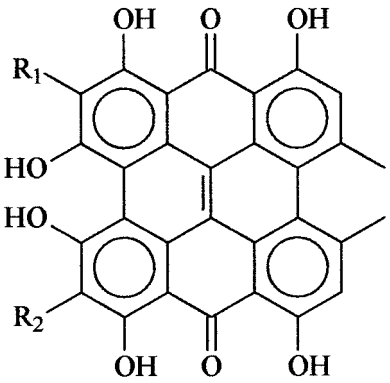

	R_1	R_2
hypercin	H	H
mono-iodohypericin	I	H
di-iodohypericin	I	I

Figure 1. Chemical structure of hypericin, mono-iodohypericin and di-iodohypericin.

of the compound is crucial for a diffusion into tumor tissue to take place.

Solid tumors grow in a three-dimensional (3-D) spatial array, and the cells in these tumors are exposed to nonuniform distributions of oxygen and nutrients as well as other physical and chemical stress. Consequently, because of the great micro-environmental variations present in different regions of tumors, significant cellular heterogeneity may result. In an attempt to design more suitable *in vitro* systems that take into consideration the 3-D arrangement of solid tumors, 3-D multicellular tumor spheroids have been developed. In fact, tumor spheroids represent quite realistically the 3-D growth and organization of solid tumors and consequently simulate much more precisely the cell–cell interactions and microenvironmental conditions found in the tumors (20–22).

In the present study the *in vitro* cellular accumulation and diffusion of hypericin in two-dimensional (2-D) and 3-D cultured RT-112 transitional cell carcinoma (TCC) cells of the bladder were studied. In addition, two iodinated derivatives of hypericin were synthesized and incorporated in the experimental work. The rationale of using the hypericin congeners is dual. First of all, it is of interest to investigate whether the iodinated hypericins with their increased lipophilicity (23) display a different biological behavior. Moreover, because the heavy-atom effect of halogen substituents facilitates the intersystem crossing between the singlet and the triplet state of a photosensitizer (24,25), the iodinated hypericin derivatives were supposed to demonstrate an optimized photodynamic effect. The outcome might therefore be of major importance when clinical PDT against superficial bladder cancers with hypericin and analogs is considered. Because many of the differences in response to PDT between cells grown in monolayer and those found in *in vivo* tumors may be the direct result of the differences in spatial organization and cell–cell contacts, photodynamic treatment with the three photosensitizers was performed using both monolayer cells and spheroids.

MATERIALS AND METHODS

Photosensitizers. Hypericin was synthesized from emodin anthraquinone according to Falk and Oberreiter (26). Briefly, emodin (2.5 ***g***), isolated from cortex Frangulae, was dissolved in 125 mL acetic acid and reduced with 5 g $SnCl_2 \cdot 2H_2O$ in 65 mL concentrated hydrochloric acid. After refluxing the mixture for 3 h at 120°C, emodin anthrone was precipitated by cooling to room temperature. To prepare protohypericin via oxidative dimerization, 2.0 g emodin anthrone was dissolved in 44 mL pyridine–piperidine (10:1), and 4 mg pyridine-1-oxide and 100 mg $FeSO_4 \cdot 7H_2O$ were added. The reaction mixture was heated at 100°C for 1 h under nitrogen in dark conditions. Protohypericin was precipitated in hexane and purified with silica column chromatography (mobile phase: ethylacetate–water with increasing amounts of acetone). A Sephadex LH-20 column (Pharmacia, Uppsala, Sweden) was used for further purification with dichloromethane, acetone and methanol as eluents. The compound was irradiated in acetone with a halogen lamp (500 W) to undergo an oxidative photocyclization reaction to form hypericin ($\varepsilon_{EtOH,592}$: 45.000 M^{-1}/cm).

Mono- and di-iodohypericin (Fig. 1) were synthesized from hypericin. Briefly, to 11 mL of a 1 mg/mL solution of NaI in 0.01 *M* NaOH were successively added 150 mL of the ethanolic hypericin solution (0.5 mg/mL), 25 mL of 0.5 *M* H_3PO_4, 50 mL of 0.2 *M* peracetic acid and 50 mL EtOH. After stirring for 30 min, the reaction was stopped by solid phase extraction of the reaction mixture on octadecylsilyl silica gel (LiChroprep® [mean particle size 20 μm, mean pore diameter 100 Å], Merck, Darmstadt, Germany). Purification of the reaction mixture was carried out using medium–performance liquid chromatography (MPLC) with EtOH–0.05 *M* NH_4OAc (70:30, vol/vol) as the eluent. The MPLC system consisted of a pump (model B-688, Büchi, Flawil, Switzerland) and a column filled with octadecylsilyl silica gel (LiChroprep®). The fractions containing pure mono–iodohypericin ($\varepsilon_{EtOH,595}$: 38.000 M^{-1}/cm) or di-iodohypericin ($\varepsilon_{EtOH,598}$: 34.000 M^{-1}/cm) (as determined by mass spectrometry) were dried by solid phase extraction on a high-capacity C18 column (Alltech® Extract Clean [bed weight 10 g, mean particle size 50 μm, mean pore diameter 60 Å], Alltech, Deerfield, IL). Further details of the synthesis will be published elsewhere.

The relative lipophilic–hydrophilic balance of hypericin and its iodinated analogs was assessed by means of reversed phase high-performance liquid chromatography (RP-HPLC) on an RP C18 column (Xterra™ [C18, mean particle size 5 μm], Waters, Milford, U.S.A) with EtOH–0.05 M NH_4OAc (85:15, vol/vol) as eluent at a flow rate of 1 mL/min and absorption monitoring at 254 nm.

All manipulations with the photosensitizers were performed under strictly subdued light conditions (<1 μW/cm^2).

2-D cell culture. RT-112, a human, moderately differentiated, non-invasive papillary TCC cell line, was obtained from the German Collection of Microorganisms and Cell Cultures (DSMZ, Braunschweig, Germany). Cells were cultured as a monolayer in minimum essential medium (MEM) with Earle's salts containing 2 m*M* L-glutamine under 5% CO_2 at 37°C. The medium was supplemented with 10% (vol/vol) fetal calf serum (FCS), 1% (vol/vol) nonessential amino acids, 1% (vol/vol) antibiotic–antimycotic solution (GIBCO-BRL, Paisley, Scotland) and tylosine (60 μg/mL) (Eli Lilly, Brussels, Belgium).

3-D cell culture. Spheroids were initiated by inoculating 5×10^3 RT-112 cells in 200 μL culture medium with 1% sodium pyruvate (100 μ*M*) (GIBCO-BRL) on 96-well tissue culture plates (Costar, Cambridge, MA) that had been underlayed previously with 1.5% agarose (Sigma, Steinheim, Germany) in MEM. The medium was replaced twice a week and after 7 days of incubation, spheroids with diameters between 450 and 500 μm were obtained, which were used for all experiments.

Average cellular accumulation. For determining the average cellular accumulation under 2-D conditions, RT-112 cells were seeded onto 6-well tissue culture plates at 9×10^5 cells per well and incubated for 24 h at 37°C. Subsequently, the medium was replaced with fresh medium containing hypericin, mono–iodohypericin or di-iodohypericin, and the cells were further incubated at 37°C for 2 h (photosensitizer concentration: 10 μ*M*) or 24 h (1 and 10 μ*M*). After incubation the cells were washed twice with phosphate-buffered saline (PBS) (GIBCO-BRL) and harvested by treatment with trypsin solution (GIBCO-BRL). The cell suspension was then pelleted by centrifugation (5 min, 600 ***g***), and the photosensitizer was extracted twice with 0.5 mL methanol–ethylacetate (50:50, vol/vol). After centrifugation (5 min, 6000 ***g***), the supernatant was concentrated under vacuum. The residue was dissolved in 200 μL dimethylsulfoxide (DMSO) and

transferred to a 96-well tissue culture plate. For determining the average cellular accumulation under 3-D conditions, spheroids were picked from the agarose culture plates and incubated in a 6-well plate (80 spheroids per well) with the different photosensitizers, as mentioned under the 2-D conditions. Subsequently, the spheroids were washed twice with PBS and incubated for 10 min with trypsin solution with shaking. The extraction was performed as described. The photosensitizer content was determined using a microplate fluorescence reader (FL600, Biotek, Winooski, VT). The excitation and emission filters were 590/20 and 645/40 nm, respectively. The number of cells per condition was determined using a Coulter Z1 particle counter (Coulter Electronics, Luton, UK). The results were calculated assuming a mean volume of 3 μL per 10^6 cells (27). All experiments were performed in triplicate.

Intraspheroidal fluorescence distribution and quantification. Spheroids were incubated with the individual photosensitizers for 2 h (10 μ*M*) or 24 h (1 and 10 μ*M*), after which they were transferred into Tissue Tek embedding medium (Miles, Elkhart, IN) and immersed in liquid nitrogen. Cryostat microtomy was performed to section at 5 μm thickness. Centrally cut sections were examined by fluorescence microscopy (Axioskop 2 plus fluorescence microscope, Carl Zeiss, Göttingen, Germany) using a 535/25 nm band-pass excitation filter and a 590 nm long-pass emission filter. Fluorescence images were acquired using a light-sensitive charge-coupled device digital camera (AxioCam HR, Carl Zeiss). A KS imaging software system (Carl Zeiss, Vision, Hallbergmoos, Germany) was used to measure the average fluorescence in concentric layers of 5.3 μm thickness from the rim to the center (2.6 μm in the case of di-iodohypericin). Fluorescence intensities were determined as the mean of eight spheroids. Corrections were made for autofluorescence. The concentration of the photosensitizer from the rim (C_{max}) to the center (C_{min}) of the spheroid was calculated according to the equation

$$C_{r_1,r_2} = \frac{V_s \times C}{d} \int_{r1}^{r2} F(r)dr$$

where C_{r_1,r_2} is the concentration of the photosensitizer in a specific layer of the spheroid, r is a point on the radius of the spheroid, V_S is the spheroid volume, C is the average cellular accumulation extracted, d is the thickness of the cryostat section and $F(r)$ is the equation of the fitted fluorescence decay curve. After curve fitting using nonlinear regression (Prism, San Diego, CA), CD_{50} values were determined. These values correspond to the distance along the radius (from rim to center of the spheroid) at which the photosensitizer concentration drops to half its maximal value.

Optimal PDT wavelength determination. The optimal wavelength for PDT was determined for the individual photosensitizers. Therefore, 5×10^3 cells were seeded onto 96-well tissue culture plates and incubated for 24 h at 37°C. After incubation with hypericin, mono–iodohypericin or di-iodohypericin (10 μ*M*) for 2 h, cells were exposed to 1 mW/cm^2 light irradiation at different wavelengths ranging from 585 to 610 nm for 3 min (5 min in the case of di-iodohypericin). For irradiation, light emitted by a Rhodamine 6G dye laser (375B, Spectra Physics, Mountain View, CA) pumped by a 4 W argon laser (Spectra Physics) was coupled into a fiber optic microlens (Rare Earth Medical, West Yarmouth, MA) to obtain an ultrauniform intensity distribution. The fluence rate at the surface of the tissue culture plate was measured with an IL 1400 radiometer (International Light, Newburyport, MA). After 2 days the surviving fraction was determined with a 3-(4,5-dimethylthiazol-2-yl)-2,5-diphenyl-tetrazolium bromide (MTT) proliferation assay, based on the ability of mitochondrial enzymes to reduce MTT (Sigma) into purple formazan crystals. For this purpose, the medium was replaced by a 1 mg/mL MTT solution in fresh medium followed by incubation for 4 h. The MTT solution was then removed and replaced with 200 μL DMSO. The concentration of formazan per well was determined by measuring its absorbance at 550 nm using a microplate reader. The surviving fraction, according to the concentration obtained with nontreated cells, was calculated from three replicates.

Photodynamic treatment. For determining the photocytotoxic effect under 2-D conditions, RT-112 cells were seeded onto 96-well tissue culture plates at 5×10^3 cells per well. After 24 h incubation the medium was replaced with fresh medium containing 125 n*M*, 1 μ*M* or 10 μ*M* hypericin, mono–iodohypericin or di-iodohypericin, and the cells were incubated under dark conditions at 37°C for 2 or 24 h. The cells were washed twice with PBS and irradiated for 3 or 30 min with a light dose of 1.8 J/cm^2. For each compound the photocytotoxic experiments were performed at the optimal wavelength. The cells were further cultured for 2 days. For determining the photocytotoxic effect under 3-D conditions, spheroids (eight per well) were analogously incubated, washed and irradiated in a 24-well tissue culture plate. Immediately after PDT, spheroids were dissociated into a single-cell suspension with trypsin solution. Once the dissociation was complete, trypsin was inactivated by adding an equal volume of medium. The dissociated cells were centrifuged (5 min, 600 ***g***) and resuspended in fresh medium. An appropriate number of cells from control and PDT groups were resuspended in 200 μL medium and cultured for 2 days in a 96-well tissue culture plate in the dark. Cell proliferation was determined with the MTT proliferation assay. The surviving fraction was calculated from three replicates. The control group consisted of 2-D or 3-D cultured cells that were incubated with photosensitizer but were protected from light or that were irradiated in the absence of a photosensitizer.

RESULTS

HPLC retention time

To assess the relative hydrophilic–lipophilic character of hypericin and its iodinated analogs, their retention times were determined on an RP-HPLC (C-18) column. The retention times were 9.2, 13.3 and 20.3 min for hypericin, mono–iodohypericin and di-iodohypericin, respectively.

Spheroid growth

Spheroids were sized three times a week. Mean diameter and standard deviation (SD) were calculated (n = 16). Cells initially conjoined to a diameter of 425 ± 9 μm. The spheroid growth was exponential during the first 8 days, followed by a linear phase. After 16 days a steady state in size was reached (Fig. 2). For experiments, spheroids with a diameter of 450–500 μm were used, corresponding to 7 days in culture.

Average cellular accumulation

Figure 3 shows the average accumulation of photosensitizer in RT-112 monolayer cells and spheroids after 2 or 24 h incubation, as a function of the initial extracellular concentrations applied. The final intracellular amount was converted to micromolar units assuming 3 μL as the mean volume of 10^6 cells. As can be seen, the average cellular uptake in monolayer cells and spheroids augmented dramatically by increasing the extracellular concentration up to 10 μ*M* and by prolonging the incubation time from 2 to 24 h. The difference in average cellular accumulation between hypericin and mono–iodohypericin was not significant, based on the one-way analysis of variance (ANOVA) with Tukey–Kramer post test ($P > 0.05$), both in monolayers and in spheroids. On the other hand, di-iodohypericin exhibited a significantly increased average uptake ($P < 0.05$) compared with hypericin and mono–iodohypericin. For instance, after 24 h of incubation with a 10 μ*M* concentration, di-iodohypericin accumulated 1.3 and 2.5 times more in monolayer cells and spheroids, respectively, as compared with hypericin. In all cases the photosensitizers concentrated dramatically more in monolayers than in spheroids. After incubation of 10 μ*M* hypericin for 24 h, the intracellular accumulation in monolayer cells was 10.3 times higher than in spheroids. For mono–iodohypericin and di-iodohypericin the ratios were 8.7 and 5.2, respectively.

Intraspheroidal fluorescence distribution and quantification

Furthermore, the extent of photosensitizer distribution and penetration into the spheroids was examined. Therefore, centrally cut cryostat cross-sections were analyzed by fluorescence micros-

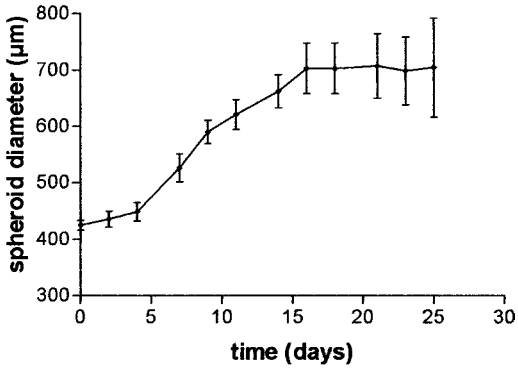

Figure 2. Growth of spheroids of RT-112 TCC cells. Mean ± SD (n = 16).

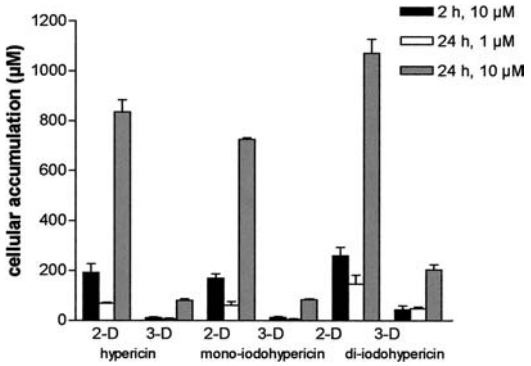

Figure 3. The effect of photosensitizer concentration and incubation time on average uptake in RT-112 monolayer cells (2-D) and spheroids (3-D). The final intracellular amount was converted to micromolars assuming 3 µL as the mean volume of 10^6 cells. Mean ± SD (n = 3).

copy. Figure 4 shows a fluorescence photomicrograph of a section of an RT-112 spheroid after a 2 h incubation period with 10 µ*M* hypericin (Fig. 4A) or a 24 h incubation period with mono-iodohypericin (Fig. 4B) or di-iodohypericin (Fig. 4C). An imaging software system was used to measure the mean fluorescence from the rim to the center. From these data the actual concentrations of the photosensitizer throughout the spheroid were calculated (Table 1, Fig. 5). CD_{50} values corresponding to the distance along the radius at which the concentration drops to half its maximal value were also determined (Table 1, Fig. 5). These values are indicative of the relative penetration of a photosensitizer. In the case of hypericin and its mono–iodo derivative, a typical pattern can be seen with a high concentration at the periphery declining rapidly and reaching a steady-state situation at about 75–100 µm below the surface. Prolonging the incubation time from 2 to 24 h (10 µ*M*) resulted in an overall increased concentration that was 6.4 and 7.2 times higher at the spheroid rim and 4.0 and 6.8 times higher in the central region for hypericin and mono–iodohypericin, respectively. Also, the relative penetration improved, as reflected by the higher CD_{50} values. Similar effects were seen by increasing the extracellular concentration from 1 up to 10 µ*M* (24 h incubation) (Table 1, Fig. 5). In general, hypericin and mono–iodohypericin behaved similarly (Table 1).

Conversely, accumulation of di-iodohypericin was restricted to the very outer layers of the spheroid (CD_{50} values: 1.3–1.7 µm), and virtually no compound was present 2.6 and 10.4 µm below the surface for a 2 and 24 h incubation (10 µ*M*), respectively. Prolonging the incubation time resulted in a higher concentration of di-iodohypericin only at the outer rim.

Optimal wavelength determination

PDT at different wavelengths had a dramatic influence on the treatment outcome (Fig. 6). The photocytotoxicity of RT-112 cells at various wavelengths closely follows the absorption spectrum in PBS with 10% FCS with absorption maxima at 595, 598 and 601 nm for hypericin, mono–iodohypericin and di-iodohypericin, respectively (data not shown). Based on these results, the absorption maximum for each compound was selected as its activating wavelength for PDT.

Antiproliferative assay

To investigate the photocytotoxic effect, monolayers and spheroids were incubated for 2 or 24 h with three different concentrations of photosensitizer and subjected to a light dose of 1.8 J/cm^2 using two different light regimes. The cells were then further incubated for 2 more days in the dark without photosensitizer, after which the surviving fraction was determined. The results of irradiation with 10 mW/cm^2 for 3 min are shown in Fig. 7A for 2-D and Fig. 7B for 3-D cultures. As expected, prolonging the incubation time and increasing the concentration of the photosensitizer led to enhanced photocytotoxicity. The data further illustrate that hypericin and mono–iodohypericin had a far more potent photodependent antiproliferative effect in comparison to di-iodohypericin both on spheroids and especially on cell monolayers. Moreover, the photocytotoxic effect on spheroids in general was dramatically lower for all three photosensitizers. The photocytotoxic effect of the photosensitizers on monolayer cells was virtually independent of the light regime used (10 mW/cm^2 for 3 min vs 1 mW/cm^2 for 30 min) (results not shown). However, in the case of spheroids the lower fluence rate was slightly more effective at least when the highest concentration of the photosensitizers in combination with 24 h incubations were used. For instance, a survival fraction of 2.2% was seen for hypericin, whereas in the case of the higher fluence rate this amounted to 18.5%.

It should further be mentioned that no cytotoxic effects were observed under control conditions.

DISCUSSION

The present work was undertaken to investigate the accumulation and penetration of hypericin and two iodinated derivatives in 2-D and 3-D cultured RT-112 TCC cells of the bladder and to compare

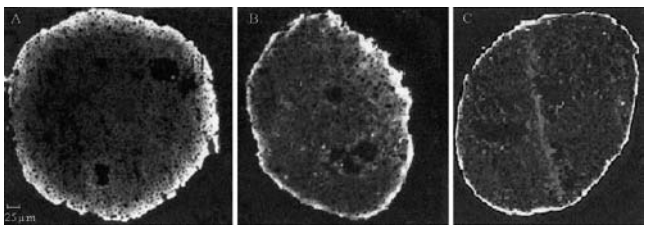

Figure 4. Fluorescence photomicrographs of RT-112 spheroids after 2 h of incubation with 10 µ*M* hypericin (A) and 24 h of incubation with mono–iodohypericin (B) or di-iodohypericin (C). Because of the lower fluorescence yields of the iodinated derivatives, photomicrographs were taken with different sensitivities.

Table 1. Maximum and minimum concentration (C_{max} and C_{min}, respectively) (in μ*M*) and distance along the radius (from rim to center of the spheroid) at which the concentration drops to half its maximal value (CD_{50}), as a function of concentration and incubation time. Spheroids were incubated with photosensitizer for 2 h (10 μ*M*) or 24 h (1 and 10 μ*M*). Frozen sections were analyzed with fluorescence microscopy and imaging software, and the concentrations were calculated. Data represent mean (n = 8). SD < 5%*

	2 h (10 μ*M*)			24 h (1 μ*M*)			24 h (10 μ*M*)		
	C_{max}	C_{min}	CD_{50}	C_{max}	C_{min}	CD_{50}	C_{max}	C_{min}	CD_{50}
Hypericin	17.9	2.5	12.2	6.6	0.3	17.7	115	9.8	22.6
Mono–iodohypericin	18.2	2.0	13.1	10.1	0.3	14.4	130	13.8	20.5
Di-iodohypericin	696	0	1.3	ND	ND	ND	2676	0	1.7
One-way ANOVA with Tukey–Kramer post test									
Hypericin *vs* mono–iodohypericin	NS	***	NS	***	NS	***	NS	***	NS
Hypericin *vs* di-iodohypericin	***	***	***	/	/	/	***	***	***
Mono–iodohypericin *vs* di-iodohypericin	***	***	***	/	/	/	***	***	***

*ND, not detectable; NS, not significant.
***, $P < 0.001$.

their PDT potential. The electrophilic iodination at positions 2 and 5 increased the lipophilic character of hypericin, as proven by the longer retention times of the analogs on an RP-HPLC column. Furthermore, the substitution reactions resulted in small bathochromic shifts in the absorption spectra.

All compounds, especially the di-iodo analog, were readily taken up by 2-D cultured cells. For instance, incubating the cells for 24 h with the photosensitizers resulted in average cellular concentrations that were 60–80 times (hypericin, mono–iodohypericin) or 100–140 times (di-iodohypericin) higher than the extracellular concentration (1 or 10 μ*M*) used. Of importance, it has been found that the chemical characteristics of hypericin and related molecules affect the mechanism of cellular uptake. In general, their internalization and the ensuing localization into viable cells depend on passive diffusion, partitioning, endocytosis and probably pinocytosis (28). As far as hypericin is concerned, it has been shown that the compound colocalizes in the endoplasmatic reticulum and the lysosomes, in the latter case by means of a preliminary extracellular binding to low-density lipoproteins (LDL) followed by an endolysosomal internalization route (28). As the fraction of photosensitizer bound to LDL increases with increasing lipophilicity, it is speculated that the internalization of the iodinated analogs largely depends on this receptor-mediated pathway with lysosomal targeting as a result.

By means of spin-orbit coupling, heavy-atom substitutions of photosensitizers are known to increase the quantum yield of intersystem crossing and concomitantly their singlet oxygen production (29). For instance, it was found that the singlet oxygen yield of hypericin was 0.73, whereas a tetrabromoderivative of hypericin exhibited a yield as high as 0.92 (24). Therefore, because all photosensitizers show roughly similar molar absorption coefficients (see Materials and Methods), and especially because similar or higher cellular accumulations of the iodinated analogs were found as compared with the parent compound, an enhanced photocytotoxicity exerted by the analogs was expected. It turned out, however, that the mon–oiodo analog was about as potent as hypericin, whereas, even more unexpectedly, di-iodohypericin exhibited significantly less photodynamic potential. Similar inconsistencies between singlet oxygen production, cellular accumulation and photocytotoxicity have been observed with cyanine dyes (30). Because it is known that the cellular response to ROS dramatically depends on the subcellular positioning of the photosensitizer (31,32), it is anticipated that, as compared with hypericin, the lipophilic analogs display a (slightly) different subcellular distribution or a modified interaction with their molecular environment, resulting in a diminished sensitivity of the cells. With the possibility of further deciphering the relation between subcellular oxidative damage and cellular responses, an important topic in current fundamental PDT research, it will important to investigate this hypothesis in detail.

Conversely, it should be mentioned that although the MTT antiproliferative assay used in the experimental work is generally accepted as a quick and reliable measurement of the response of human tumor cells to PDT (33), a colony forming assay is a more accurate method to assess cytotoxicity (34). This method also allows long-term cellular effects to be registered, and it could be argued that the discrepancy seen is due to a relative lack of sensitivity of the MTT method for apoptotic events that initiate only 1 or 2 days after photodynamic treatment. Unfortunately, we were unable to run the clonogenic assay successfully with RT-112 because replating of the cells led to a disperse cell growth without clear colony formation or, by replating less cells, to no colony formation at all. Obviously, more work is needed that investigates specifically the biochemical and cellular responses seen as a function of time after photodynamic treatment with the different photosensitizers used.

In this study, not only PDT effects on 2-D cultured cells but also the penetration ability of the photosensitizer in tumor tissue were investigated. A largely heterogeneous distribution of the photosensitizer in malignant tissue might indeed represent an important obstacle in achieving an efficient tumor kill in clinical PDT practice. In the present work the spheroids were used as multicellular systems that mimick the histoarchitecture of transitional papillary carcinoma and flat CIS of the bladder. In combination with the use of lipophilic analogs of hypericin, it therefore became possible to investigate the importance of the lipophilic–hydrophilic character of the compounds for a prompt diffusion into tumor tissue to take place.

Fluorescence microscopic imaging of spheroids together with a detailed analysis of the data showed a typical distribution with high concentrations of the photosensitizer at the periphery decreasing rapidly to a steady-state situation in the inner spheroidal regions. Similar fluorescence patterns in spheroids are seen with *meta*-tetra-(hydroxyphenyl)chlorin, with a constant fluorescence

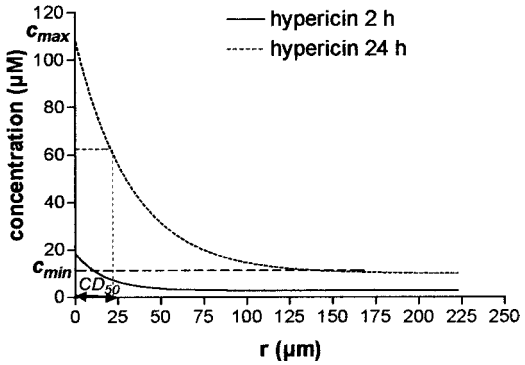

Figure 5. Exponential decline of the concentration as a function of the penetration depth along the radius (r) in spheroids after 24 h of incubation with 10 μ*M* hypericin.

value at 50 μm from the surface, which is 5- to 10-fold less than that at the periphery (35). Photofrin II on the contrary shows a good overall penetration in spheroids but a patchy distribution between cells regardless of position across the spheroid (36).

Because di-iodohypericin almost exclusively bound to the outermost part of spheroids with a very poor penetration, this compound represented an extreme case of this principle. An inverse correlation seems therefore to exist between the extent of cellular uptake under 2-D conditions and the penetration of the compounds in multicellular systems: the higher the uptake, the poorer the penetration. Likely, di-iodohypericin binds more avidly to cellular constituents, building up high concentrations at the rim and preventing any further penetration in the deeper region of the spheroid.

Conversely, when discussing the penetration of hypericins in spheroids, the presence of an extracellular matrix (ECM) should also be taken into consideration. This matrix consists of a network of structural and adhesive proteins embedded in a gel of glycosaminoglycans (GAG) and proteoglycans. ECM has been found in the urothelial lining of human bladders (37,38) and, importantly, is also expressed in spheroids but not in cells cultured in monolayers (39). Of importance, periodic acid–Schiff staining, a method widely used particularly in the demonstration of various carbohydrates, either alone or combined with other molecules such

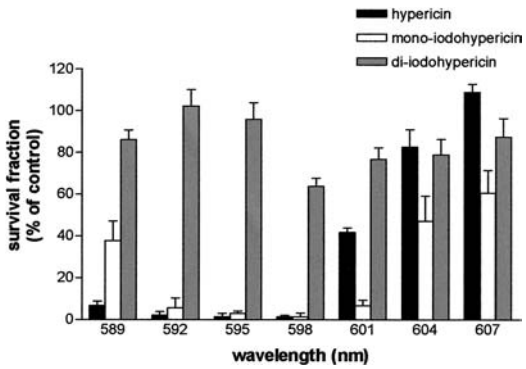

Figure 6. Survival fractions of RT-112 cells after PDT with hypericin and analogs at different wavelengths. RT-112 cells were incubated with 10 μ*M* for 2 h and exposed to light (hypericin and monoiodohypericin, 1 mW/cm^2 for 3 min; di-iodohypericin, 1 mW/cm^2 for 5 min). Data represent mean ± SD (n = 3).

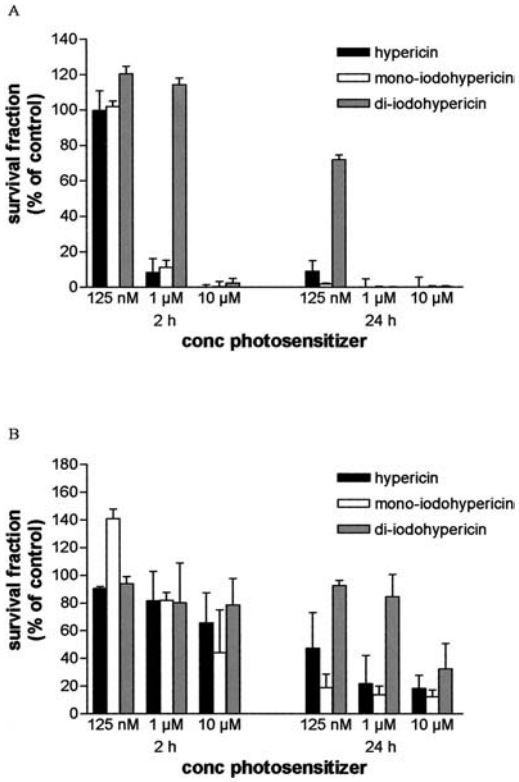

Figure 7. Survival fractions of the photosensitizers on RT-112 monolayer cells (A) and spheroids (B) after incubation for 2 or 24 h and irradiation with 10 mW/cm^2 for 3 min at 595 nm for hypericin, 598 nm for mono-iodohypericin and 601 nm for di-iodohypericin. Data represent mean ± SD (n = 3).

as proteins, was able to demonstrate a positive staining in the RT-112 spheroid. In monolayer cells, however, it was absent (results not shown). Consequently, it is presumed that the hydrophilic character and the negatively charged chains of GAG and proteoglycans hamper the penetration of the compounds, which are present as monobasic salts under physiological conditions, in the spheroid. Therefore, together with the lipophilic buffer zone, the presence of this ECM might be a possible explanation for the observed limited spheroidal uptake of hypericin and its analogs, which in general is an order of magnitude lower than in monolayer cells.

The outcome of the photocytotoxic effect in the 3-D system is compatible with the results obtained in the 2-D system, with di-iodohypericin as the least potent photosensitizer. However, the photocytotoxic effect observed with 3-D cultured cells is dramatically lower. Compared with conventional monolayer cultures, cells in 3-D aggregates resemble more closely the *in vivo* situation with regard to cell shape and cell environment. For instance, within spheroids, steep gradients exist for cellular oxygen levels, nutrients, pH and glucose concentrations, and this particular situation might affect the PDT outcome.

To determine whether oxygen depletion induced by photodynamic treatment protected cells from cytotoxic damage, two different fluence rates were used (1 and 10 mW/cm^2) while keeping the total light dose constant (1.8 J/cm^2). It was figured that by lowering the fluence rate and therefore improving the ratio between oxygen diffusion and consumption, the number of cells affected

by PDT would increase, especially in the case of spheroids (40). On the other hand, a subcellular relocalization of the photosensitizer during a 30 min light exposure could also take place, as seen for other photosensitizers (41), affecting the overall cell killing. However, only under conditions where the highest concentration of the photosensitizer in combination with a 24 h incubation was used could a small improvement in the photocytotoxic effect be observed. However, and more likely, it is presumed that especially the low concentrations of the photosensitizers typically found in the deeper layers of the spheroids fully explain the resistance of the cellular aggregates against PDT observed with the hypericins.

In summary, our results show that the iodinated analogs of hypericin do not possess a higher cytotoxic effect than hypericin upon irradiation in either monolayers or spheroids. Furthermore, our study demonstrates that although in a preclinical phase it is tempting to use monolayers as a simple way to evaluate the *in vivo* potential of newly developed photosensitizers, the use of 3-D cell aggregates resembling the *in vivo* situation much better is critical for a correct evaluation of their efficacy.

Acknowledgements—We thank Paula Aertsen and Lydie Vanrykel (Department of Pathology) for excellent technical assistance. This work was supported by grants awarded by Fonds voor Wetenschappelijk Onderzoek-Vlaanderen (FWO Vlaanderen), the Onderzoeksfonds of K.U. Leuven (Onderzoekstoelage), and a Geconcerteerde Onderzoeksactie (GOA) of the Flemish Government.

REFERENCES

1. Dougherty, J. T., J. C. C. Gomer, B. W. Henderson, G. Jori, D. Kessel, M. Korbelik, J. Moan and Q. Peng (1998) Photodynamic therapy. *J. Natl. Cancer Inst.* **90**, 889–905.
2. Ochsner, M. (1997) Photophysical and photobiological processes in the photodynamic therapy of tumours. *J. Photochem. Photobiol. B: Biol.* **39**, 1–18.
3. Fabris, C., G. Valduga, G. Miotto, L. Borsetto, G. Jori, S. Garbisa and E. Reddi (2001) Photosensitization with zinc(II) phthalocyanine as a switch in the decision between apoptosis and necrosis. *Cancer Res.* **61**(20), 7498–7500.
4. Zimmermann, A., M. Ritsch-Marte and H. Kostron (2001) mTHPC-mediated photodynamic diagnosis of malignant brain tumors. *Photochem. Photobiol.* **74**(4), 611–616.
5. Battah, S. H., C. E. Cheen, H. Nakanishi, S. Gerscher, A. J. MacRobert and C. Edward (2001) Synthesis and biological studies of 5-aminolevulinic acid-containing dendrimers for photodynamic therapy. *Bioconjug. Chem.* **12**(6), 980–988.
6. Matroule, J. Y., C. M. Carthy, D. J. Granville, O. Jolois, D. W. Hunt and J. Piette (2001) Mechanism of colon cancer cell apoptosis mediated by pyropheophorbide-a methylester photosensitization. *Oncogene* **20**(30), 4070–4084.
7. Fox, F. E., Z. Niu, A. Tobia and A. H. Rook (1998) Photoactivated hypericin is an anti-proliferative agent that induces a high rate of apoptotic death of normal, transformed and malignant T lymphocytes: implications for the treatment of cutaneous lymphoproliferative and inflammatory disorders. *J. Investig. Dermatol.* **111**, 327–332.
8. Johnson, S. A., A. E. Dalton and R. S. Pardini (1998) Time-course of hypericin phototoxicity and effect on mitochondrial energies in EMT6 mouse mammary carcinoma cells. *Free Radic. Biol. Med.* **25**, 144–152.
9. Vandenbogaerde, A. L., E. M. Delaey, A. M. Vanthiegem, B. E. Himpens, W. J. Merlevede and P. A. de Witte (1998) Cytotoxicity and anti-proliferative effect of hypericin and derivatives after photosensitization. *Photochem. Photobiol.* **67**, 119–125.
10. Vandenbogaerde, A. L., K. R. Geboes, J. F. Cuveele, P. M. Agostinis, W. J. Merlevede and P. A. de Witte (1996) Antitumour activity of photosensitized hypericin on A431 cell xenografts. *Anticancer Res.* **16**, 1619–1625.
11. Chen, B. and P. A. de Witte (2000) Photodynamic therapy efficacy and tissue distribution of hypericin in a mouse P388 lymphoma tumor model. *Cancer Lett.* **150**, 111–117.
12. Lavie, G., Y. Mazur, D. Lavie and D. Meruelo (1995) The chemical and biological properties of hypericin: a compound with a broad spectrum of biological activities. *Med. Res. Rev.* **15**, 111–119.
13. Jardon, P., N. Lazorchak and R. Gautron (1986) Propriétés du premier état triplet de l'hypericine étude par spectroscopie laser. *J. Chim. Phys.* **83**, 311–315.
14. Racinet, H., P. Jardon and R. Gautron (1988) Formation d'oxygène singulet photosensibilisée par l'hypericine étude cinétique en milieu micellaire non ionique. *J. Chim. Phys.* **85**, 971–977.
15. Duran, N. and P. S. Song (1986) Hypericin and its photodynamic action. *Photochem. Photobiol.* **43**, 677–680.
16. Kraus, G. A., W. J. Zhang, M. J. Fehr, K. W. Petrich, Y. Wannemuehler and S. Carpenter (1996) Research at the interface between chemistry and virology: development of a molecular flashlight. *Chem. Rev.* **1**, 523–535.
17. Diwu, Z. and J. W. Lown (1993) Photosensitization with anticancer agents. 17. EPR studies of photodynamic action of hypericin: formation of semiquinone radical and activated oxygen species on illumination. *Free Radic. Biol. Med.* **14**, 209–215.
18. D'Hallewin, M. A., P. A. de Witte, E. Waelkens, W. Merlevede and L. Baert (2000) Fluorescence detection of flat bladder carcinoma in situ after intravesical instillation of hypericin. *J. Urol.* **164**, 349–351.
19. D'Hallewin, M. A., A. R. Kamuhabwa, T. Roskams, P. A. M. de Witte and L. Baert (2002) Hypericin-based fluorescence diagnosis of bladder carcinoma. *BJU Int.* **89**, 760–763.
20. Kunz-Schughart, L. A., M. Kreutz and R. Knuechel (1998) Current status review: multicellular spheroids: a three-dimensional in vitro culture system to study tumour biology. *Int. J. Exp. Pathol.* **79**, 1–23.
21. Mueller-Klieser, W. (1987) Guest editorial: multicellular spheroids: a review on cellular aggregates in cancer research. *J. Cancer Res. Clin. Oncol.* **113**, 101–122.
22. Hamilton, G. (1998) Multicellular spheroids as an in vitro tumor model. *Cancer Lett.* **131**, 29–34.
23. Obermüller, R. A., K. Hohenthanner and H. Falk (2001) Toward hypericin-derived potential photodynamic therapy agents. *Photochem. Photobiol.* **74**, 211–215.
24. Delaey, E., I. Zupko, B. Chen, A. Derycke, F. Van Laar D. De Vos and P. A. de Witte (2003) Comparison of hexamethylhypericin and tetrabromohypericin to hypericin for their *in vivo* efficacy as PDT tools. *Int. J. Oncol.* **23,** 519–524.
25. Falk, H. and W. Schmitzberger (1993) On the bromination of hypericin: the gymnochrome chromophores. *Monatsh. Chem.* **124**, 77–81.
26. Falk, H. and M. Oberreiter (1993) A convenient semisynthetic route to hypericin. *Monatsh. Chem.* **124**, 339–341.
27. Lin, C. W., J. R. Shulok, Y. K. Wong, C. F. Schanbacher, L. Cincotta and J. W. Foley (1991) Photosensitization, uptake and retention of phenoxazine Nile blue derivatives in human bladder carcinoma cells. *Cancer Res.* **51**, 1109–1116.
28. Siboni, G., H. Weitman, D. Freeman, Y. Mazur, Z. Malik and B. Ehrenberg (2002) The correlation between hydrophilicity of hypericins and helianthrone: internalization mechanisms, subcellular distribution and photodynamic action in colon carcinoma cells. *Photochem. Photobiol. Sci.* **1**, 483–491.
29. Atkins. P. W. (1994) Spectroscopy 2: electronic transitions. In *Physical Chemistry*, (J. Crowe, ed.) p. 599. Oxford University Press Oxford, U.K.
30. Delaey, E. M., F. van Laar, D. de Vos, A. Kamuhabwa, P. Jacobs and P. A. M. de Witte (2000) A comparative study of the photosensitizing characteristics of some cyanine dyes. *J. Photochem. Photobiol.* **55B**, 27–36.
31. Agostinis, P., A. Vanthiegem, W. Merlevede and P. A. M. de Witte (2002) Review: hypericin in cancer treatment: more light on the way. *Int. J. Biochem. Cell Biol.* **34**, 221–241.
32. Oleinick, N. L. and H. H. Evans (1998) The photobiology of photodynamic therapy: cellular targets and mechanisms. *Radiat. Res.* **150**, S146–S156.
33. Dubessy, C., J. L. Merlin, C. Marchal and F. Guillemin (2000) Spheroids in radiobiology and photodynamic therapy. *Crit. Rev. Oncol./Hematol.* **36**, 179–192.
34. Oleinick, N. L., R. L. Morris and I. Belichenko (2002) The role of apoptosis in response to photodynamic therapy: what, where, why, and how. *Photochem. Photobiol. Sci.* **1**, 1–21.
35. Coutier, S., S. Mitra, L. N. Bezdetnaya, R. M. Parache, I. Georgakoudi, T. H. Foster and F. Guillemin (2001) Effects of fluence rate on cell survival and photobleaching in meta-tetra-(hydroxyphenyl)chlorin-photo-

sensitized Colo 26 multicell tumor spheroids. *Photochem. Photobiol.* **73**(3), 297–303.
36. West, C. M. L. (1989) Size-dependent resistance of human tumour spheroids to photodynamic treatment. *Br. J. Cancer* **59**, 510–514.
37. Wilson, C. B., J. Leopard, D. A. Cheresh and R. M. Nakamura (1996) Extracellular matrix and integrin composition of the normal bladder wall. *World J. Urol.* **14**, S30–S37.
38. De Klerk, D. P. (1985) The glycosaminoglycans of human bladder cancers of varying grade and stage. *J. Urol.* **134**, 978–981.
39. Glimelius, B., B. Norling, T. Nederman and J. Carlsson (1988) Extracellular matrices in multicellular spheroids of human glioma origin: increased incorporation of proteoglycans and fibronectin as compared to monolayer cultures. *Acta Pathol. Microbiol. Scand.* **96**, 433–444.
40. Foster, T. H., D. F. Hartley, M. G. Nichols and R. Hilf (1993) Fluence rate effects in photodynamic therapy of multicell tumor spheroids. *Cancer Res.* **53**, 1249–1254.
41. Wood, S. R., J. A. Holroyd and S. B. Brown (1997) The subcellular localization of Zn(II) phthalocyanines and their redistribution on exposure to light. *Photochem. Photobiol.* **65**, 397–402.